Molecular Biology of the Cell
Vol. 20, 3740–3750, August 15, 2009

Cadherin Adhesion Receptors Orient the Mitotic Spindle during Symmetric Cell Division in Mammalian Epithelia

Nicole den Elzen, Carmen V. Buttery, Madhavi P. Maddugoda,* Gang Ren,* and Alpha S. Yap

University of Queensland, Division of Molecular Cell Biology, Institute for Molecular Bioscience, St. Lucia, Brisbane, Queensland, 4072, Australia

Submitted January 9, 2009; Revised May 21, 2009; Accepted June 15, 2009
Monitoring Editor: Yixian Zheng

Oriented cell division is a fundamental determinant of tissue organization. Simple epithelia divide symmetrically in the plane of the monolayer to preserve organ structure during epithelial morphogenesis and tissue turnover. For this to occur, mitotic spindles must be stringently oriented in the Z-axis, thereby establishing the perpendicular division plane between daughter cells. Spatial cues are thought to play important roles in spindle orientation, notably during asymmetric cell division. The molecular nature of the cortical cues that guide the spindle during symmetric cell division, however, is poorly understood. Here we show directly for the first time that cadherin adhesion receptors are required for planar spindle orientation in mammalian epithelia. Importantly, spindle orientation was disrupted without affecting tissue cohesion or epithelial polarity. This suggests that cadherin receptors can serve as cues for spindle orientation during symmetric cell division. We further show that disrupting cadherin function perturbed the cortical localization of APC, a microtubule-interacting protein that was required for planar spindle orientation. Together, these findings establish a novel morphogenetic function for cadherin adhesion receptors to guide spindle orientation during symmetric cell division.

INTRODUCTION

Correctly oriented cell division in three-dimensional tissues relies on the precise positioning of the mitotic spindle before sister chromatid separation in anaphase (Rappaport, 1971). The mitotic spindle, in turn, responds to spatial cues, which orient it relative to the cell cortex (Ahringer, 2003; Thery and Bornens, 2006; Thery *et al.*, 2007). Much of our understanding of spindle orientation in tissue populations comes from studies of asymmetric cell division in *Drosophila* and *Caenorhabditis elegans*, where cell constituents are divided unequally between daughter cells (Doe and Bowerman, 2001; Kaltschmidt and Brand, 2002; Betschinger and Knoblich, 2004; Roegiers and Jan, 2004). In such cases, spindle orientation can be determined by cell shape, where the balance of forces on astral microtubules from the cell cortex centers the spindle along the long axis. Alternatively, specific molecular cues that localize to the cortex via polarity factors are hypothesized to act by binding astral microtubules or by exerting pulling or pushing forces on the spindle.

Cells in simple polarized epithelia, however, must divide symmetrically within the plane of the monolayer (Fleming *et al.*, 2007); failure to achieve this is predicted to cause cells to grow out of the monolayer, disrupting tissue architecture (Baena-Lopez *et al.*, 2005). Symmetric division requires that mitotic spindles be stringently oriented in the Z-axis, so that the division plane between daughter cells is perpendicular to the plane of the monolayer. However, little is known about the spatial cues that might instruct spindle orientation in the Z-axis in symmetrically dividing cells. Studies using isolated mammalian epithelial cells identified roles for cell shape (O'Connell and Wang, 2000) and the extracellular matrix (ECM; Thery *et al.*, 2005) in orienting spindles in the XY-plane. Integrin adhesion also affects Z-axis orientation in isolated nonpolarized cells (Toyoshima and Nishida, 2007). But these reports did not address how spindles become oriented in the Z-axis when polarized cells are organized into coherent populations. Therefore, in this study, we sought to identify spatial cues that orient the mitotic spindle in the Z-axis to thereby ensure the formation of organized epithelial sheets.

This article was published online ahead of print in *MBC in Press* (http://www.molbiolcell.org/cgi/doi/10.1091/mbc.E09–01–0023) on June 24, 2009.

* These authors contributed equally to this work.

Address correspondence to: Alpha S. Yap (a.yap@uq.edu.au).

MATERIALS AND METHODS

Cell Culture and Transfection

Madin-Darby canine kidney (MDCK) cells were cultured in DMEM with 10% fetal bovine serum; MCF10A cells in 1:1 DMEM/Ham's F-12 medium with 5% donor horse serum, 20 ng/ml epidermal growth factor, 100 ng/ml cholera toxin, 0.5 mg/ml hydrocortisone, and 10 mg/ml insulin; and human E-cadherin Chinese hamster ovary (hE-CHO) cells in Ham's F-12 medium with 10% fetal bovine serum and 12.5 mg/ml puromycin. All media were supplemented with nonessential amino acids and 2 mM L-glutamine. hE-CHO cells stably expressing human E-cadherin have been described previously (Kovacs *et al.*, 2002b). MDCK cell lines stably expressing GFP-DN E-cadherin, human E-cadherin-green fluorescent protein (GFP), or GFP alone were made by transfecting MDCK cells with cDNA constructs using Lipofectamine 2000 (Invitrogen, Carlsbad, CA). After 2 d, cells were grown under G418 selection (0.5 mg/ml), and then stable transfectants were isolated after 10–14 d by FACS of individual cells into 24-well plates. Clones were screened for expression levels by immunofluorescence and Western analysis.

Cell Synchronization

hE-CHO cells were plated at a confluency of 10% and incubated for 24 h, followed by incubation in serum-free medium for a further 24 h to synchronize cells in G0. Cells were then incubated in complete medium containing 2 mM thymidine (Sigma-Aldrich, St. Louis, MO) or 5 μg/ml aphidicolin (Sig-

ma-Aldrich) for 12 h to arrest cells at the beginning of S phase. Cells were released from S phase with two PBS washes and incubated in complete medium for 8 h to allow entry into late G2 phase/mitosis.

Plasmid Constructs

GFP-DN E-cadherin was constructed by inserting an XmaI-XbaI fragment of human E-cadherin cDNA encoding the C-terminal 134 amino acids of the cytoplasmic tail into pEGFP-C3 (Clontech). pEGFP-C3 was used as a GFP control. pCDNA3-human E-cadherin-GFP has been previously described (Miranda *et al.,* 2001).

RNA Interference

MDCK cells were plated at 8×10^3 cells/cm^2 and grown overnight, followed by transfection with duplexed small interfering RNA (siRNA) oligonucleotides (25 nM for E-cadherin, 50 nM for cadherin-6) using Lipofectamine 2000 or Lipofectamine RNAiMAX (Invitrogen). Transfection in the absence of RNA was used as a negative control. The following oligonucleotides were used: canine E-cadherin oligonucleotides (Ambion, Austin, TX): sense strand 5′-GCAUGGACUCAGAAGACAGtt-3′ and antisense strand 5′-CUGUCUUCUGAGUCCAUGCtg-3′; and canine cadherin-6 oligonucleotides (Invitrogen): sense strand 5′-UGCGGCUACAGUCAGAAUUtt-3′ and antisense strand 5′-AAUUCUGACUGUAGCCGCAtt-3′. siRNA directed against adenomatous polyposis coli (APC) were designed based on previously published sequences (Grohmann *et al.,* 2007). Cells were analyzed 2 d after transfection, except for APC depletion where cells were transfected a second time after 2 d and examined 4 d afterward. All cell dimension and spindle angle calculations were performed on cells with no detectable E-cadherin or cadherin-6 or APC by immunofluorescence staining.

Perturbing Cell–Cell Adhesion

MDCK cells grown on glass coverslips to 100% confluence were washed twice with, then incubated in, Hank's balanced salt solution (HBSS, Sigma) containing 15 mM HEPES, pH 7.4, and either 30 μM $CaCl_2$ (reduced calcium) or 1.8 mM $CaCl_2$ (control) for 1.5 h at 37°C. MCF10A cells grown on glass coverslips to 80–100% confluence were similarly treated with HBSS containing 15 mM HEPES, pH 7.4, and either 0 or 1.8 mM $CaCl_2$ for 2 h at 37°C. For E-cadherin function-blocking antibody experiments, MCF10A cells were incubated in the absence of $CaCl_2$ as above to disrupt cell–cell contacts, followed by incubation for 5 h at 37°C in complete medium either lacking or containing mouse mAb SHE78-7 (4 mg/ml; Zymed Laboratories, South San Francisco, CA) directed against the human E-cadherin ectodomain.

E-Cadherin–mediated Cell Attachment to Substrata

Recombinant hE/Fc consisting of the ectodomain of E-cadherin fused to the Fc portion of IgG was purified and adsorbed to cover slips, as previously described (Kovacs *et al.,* 2002b). To harvest mitotic hE-CHO cells, late G2 phase/mitosis-synchronized hE-CHO cultures were gently washed with HBSS/Ca, and then mitotic cells were shaken off by vigorous tapping. Alternatively, synchronized cells were harvested by treatment with 0.01% crystalline porcine trypsin (Sigma) in HBSS/Ca for 5 min at 37°C, followed by centrifugation at 1500 rpm for 3 min and resuspension in 1 ml HBSS/Ca. Cells were then seeded onto hE/Fc- and BSA-treated coverslips and incubated at 37°C for 1.5 h.

Western Analysis

Cells were lysed in 1× SDS-PAGE sample buffer (50 mM Tris.Cl, pH 6.8, 100 mM DTT, 2% SDS, 0.1% bromophenol blue, and 10% glycerol), and extracts were incubated at 100°C for 5 min. Proteins were separated by SDS-PAGE, transferred to nitrocellulose, and probed with appropriate primary and HRP-tagged secondary antibodies in 5% skim milk powder in 0.1% Tween-20/PBS solution, followed by detection by chemiluminescence. The following primary antibodies were used: mouse antibody to E-cadherin cytoplasmic tail (BD Biosciences, San Jose, CA, 1:100); rabbit anti-pan-cadherin (PEP-1, a gift from B. Gumbiner, University of Virginia, 1:2000); rabbit anti-cadherin-6 (gift from R. M. Mège, INSERM, Paris, France, 1:5000); mouse anti-β-catenin (BD Biosciences, 1:2000); rabbit anti-α-catenin (Zymed Laboratories, 1:500); rabbit anti-GFP (Invitrogen, 1:1000); rabbit anti-GAPDH (R&D Systems, Minneapolis, MN 1:5000); and mouse anti-β-tubulin (Sigma-Aldrich, 1:5000). HRP-tagged secondary antibodies (Bio-Rad Laboratories, Hercules, CA) were used at 1:5000.

Immunofluorescence

To stain for actin and Dlg1, cells were fixed in 4% paraformaldehyde in cytoskeletal buffer (10 mM PIPES, pH 6.8, 100 mM KCl, 300 mM sucrose, 2 mM EGTA, and 2 mM $MgCl_2$) for 30 min at room temperature, followed by permeabilization in 0.25% Triton X-100 in PBS for 5 min. For cadherin-6, cells were similarly fixed and then permeabilized in 0.5% Triton X-100 in PBS for 15 min, or, for costaining with APC, were processed according to the APC protocol. For APC immunofluorescence, cells were fixed in −20°C methanol for 5 min, followed by treatment with 0.2% Triton X-100 in PBS for 10 min. For LGN staining, cells were prepermeabilized in 1% Triton X-100 in PEM buffer (100 mM PIPES, pH 6.8, 5 mM EGTA, and 2.5 mM $MgCl_2$) at 37°C for 5 min and then fixed in 4% paraformaldehyde in PBS for 30 min at room temperature. For dynein, cells were prepermeabilized in 0.5% Triton X-100 in PHEM buffer (100 mM PIPES, pH 6.8, 25 mM HEPES, pH 7.4, 5 mM EGTA, and 2.5 mM $MgCl_2$) at 37°C for 3–5 min, followed by fixation in 3.2% paraformaldehyde in PHEM buffer for 20 min at room temperature, and then after fixation in −20°C methanol for 5 min. For all other antibodies, cells were either processed as above for costaining experiments or were fixed in −20°C methanol for 5 min. Cells were processed for immunofluorescence as previously described (Kovacs *et al.,* 2002b).

The following antibodies were used: rat antibody specific for canine E-cadherin ectodomain (DECMA-1, Sigma-Aldrich, 1:200); mouse antibody to canine E-cadherin ectodomain (3B8 hybridoma supernatant, 1:200); rat antibody to E-cadherin ectodomain (ECCD2, Zymed Laboratories, 1:200); mouse antibody to E-cadherin cytoplasmic tail (BD Biosciences, 1:100); rabbit antibody to E-cadherin cytoplasmic tail (1:200; Scott *et al.,* 2006); rabbit anti-cadherin-6 (gift from R. M. Mège, 1:500); rabbit anti-β-catenin (gift from B. Gumbiner, 1:1000); mouse anti-β-catenin (BD Biosciences, 1:100); rabbit anti-α-catenin (gift from B. Gumbiner, 1:100); mouse anti-γ-tubulin (Sigma-Aldrich, 1:200); mouse anti-Na,K-ATPase (6H, gift from M. Caplan, Yale University, 1:200); rabbit anti-claudin-4 (Zymed Laboratories, 1:25); rabbit anti-ZO-1 (Zymed Laboratories, 1:50); rabbit anti-desmoplakin (NW6, gift from K. Green, Northwestern University Feinberg School of Medicine, 1:50); rabbit anti-Par3 (Upstate Biotechnology, Lake Placid, NY, 1:200); rabbit anti-aPKCζ (Santa Cruz Biotechnology, Santa Cruz, CA, 1:200); mouse anti-Lgl1 (gift from P. Brennwald, University of North Carolina, 1:50); mouse anti-Scribble (7C6.D10, gift from P. Humbert, Peter MacCallum Cancer Centre, 1:5); mouse anti-Dlg1 (2D11, Santa Cruz Biotechnology, 1:100); rabbit anti-dynein intermediate chain (IC) (gift from K. Vaughan, University of Notre Dame, 1:100); mouse anti-p150^{Glued} (BD Biosciences, 1:25); rabbit anti-NuMA (gift from D. Compton, Dartmouth Medical School, 1:200); rabbit anti-LGN (gift from Q. Du, Medical College of Georgia, 1:200); mouse anti-APC (Ali; 1:50) and rabbit anti-APC (M-APC, 1:200; both gifts from I. Nathke, University of Dundee); rabbit anti-GFP (Invitrogen, 1:1000); and mouse anti-GFP (Invitrogen, 1:200). Actin was stained with Alexa Fluor 488- or 594-phalloidin (Invitrogen, 1:500), and DNA was stained with DAPI (20 ng/ml). Alexa Fluor–conjugated secondary antibodies (Invitrogen) were used at 1:500 throughout. Epifluorescence images were taken using an Olympus AX-70 microscope (Melville, NY) with a Hamamatsu Orca 1 CCD camera (Bridgewater, NJ) using MetaMorph imaging software (Universal Imaging, West Chester, PA). Three-dimensional Z-stacks were collected on a Zeiss LSM-510 confocal microscope (Thornwood, NY); Zeiss LSM software was used to display orthogonal views and to measure distances in three dimensions. All images were processed using Adobe Photoshop software (San Jose, CA).

Cell Dimension and Spindle Angle Measurements

Unless otherwise stated, cells were grown on glass coverslips. MDCK cells grown on polycarbonate transwell filters (0.4-μm pore size, Corning Glass Works, Corning, NY) were plated at 2×10^5 cells/cm^2 and cultured for 3 d, with a feeding every 24 h. Monolayers were methanol-fixed and stained for E-cadherin, cadherin-6 and/or β-catenin, together with γ-tubulin and DAPI to label DNA. Coverslips and filters were mounted using glass coverslip pieces and adhesive dots as spacers, respectively. Z-stacks were taken with an XY-axis resolution of 0.09 mm/pixel and a Z-axis resolution of 0.2 mm/pixel for cell height measurements and 0.32 mm/pixel for all other measurements.

For each experiment, metaphase and anaphase cells analyzed were from the same coverslip or transwell filter. Cells were defined as being in metaphase when chromosomes were aligned at the cell equator. Early anaphase was defined as that point at which sister chromatids had started to separate, but where cell elongation and membrane invagination had not yet occurred. For each metaphase cell analyzed, spindle length, average cell width, and cell height were measured. Spindle length was taken as the distance between spindle poles, marked with γ-tubulin. β-Catenin or E-cadherin staining was used to measure average cell width, taken as the mean of two perpendicular lines, one parallel to the longest cell edge, bisecting at the cell center. Height was measured from a separate Z-stack that used scattering of confocal reflected light to illuminate the entire cell. The use of light scatter to measure cell height was validated by comparison with height measurements of GFP-expressing cells using GFP fluorescence (data not shown). Mean ± SE of metaphase cell dimensions were calculated from three separate experiments, with an overall $n \geq 45$ cells.

Except in the cases of RNA interference (RNAi) experiments and isolated hE-CHO cells plated on hE/Fc-coated coverslips, where all stages of anaphase were used due to low numbers, spindle angles relative to the plane of the monolayer were calculated for cells in early anaphase before cell elongation. The distances between γ-tubulin foci in three dimensions (xyz, equals spindle length), in the XY-axis (xy) and in the Z-axis (z) were measured, giving the dimensions of a right-angled triangle between the spindle poles and a plane parallel to the coverslip (see Figure 1). The spindle angle relative to the plane of the coverslip was then calculated using $\tan^{-1}$ (z/xy) $*$ 180°/π. Mean spindle angles were calculated from data pooled from three independent experiments, each with $n \geq 30$ cells, except for Figure 1, where each $n \geq 15$ cells, and for hE-CHO cells, where each $n \geq 13$ cells. Frequency distributions

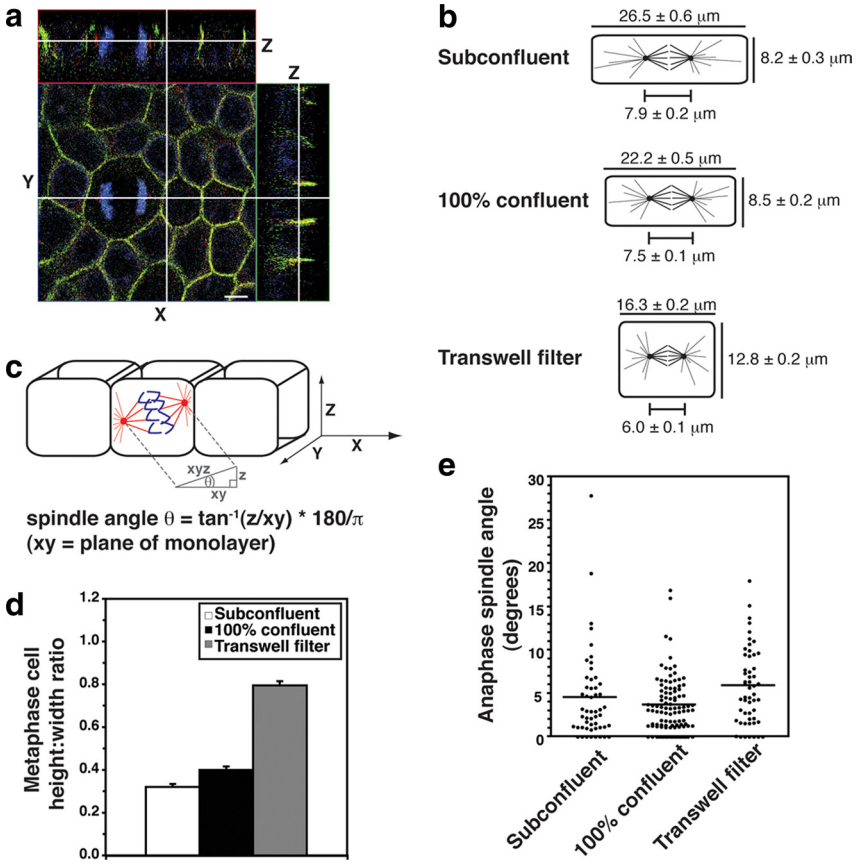

Figure 1. Spindle orientation in the plane of the monolayer does not correlate with changes in cell geometry. (a) XYZ projections of a confocal Z-stack taken of an MDCK monolayer stained for β-catenin (green), γ-tubulin (red), and DNA (blue), showing an anaphase cell dividing symmetrically. Apical is up. White lines indicate the planes at which orthogonal views were taken. Scale bar, 5 μm. (b) Schematic diagram showing metaphase cell dimensions and spindle lengths (pole-to-pole) from MDCK monolayers cultured on coverslips and grown to subconfluence or 100% confluence or grown to high density on transwell filters in order to obtain different cell geometries (mean ± SE, n ≥ 50 cells, pooled from three independent experiments). Cell dimensions were taken in metaphase, as this is when the spindle is at its longest before sister chromatid separation, and thus when any geometric constraints on spindle movements and spindle orientation would be expected to be at their greatest. (c) Diagram of how spindle angles were calculated from confocal Z-stacks. Spindles oriented parallel to the plane of the monolayer had an angle of 0°, whereas spindles perpendicular to the monolayer had an angle of 90°. (d) Metaphase cell height-width ratios from the cells in b (mean ± SE). Cell height-width ratios increased with cell confluency. (e) Spindle angles relative to the plane of the monolayer of anaphase cells from the same experiments as in b and c. In each case, the spread and overall mean of anaphase spindle angles are shown (n ≥ 50 cells). Anaphase cells were used for spindle angle measurements to avoid inaccuracies resulting from spindle orientation changes during metaphase. No correlation was found between anaphase spindle angle and cell height-width ratios (two-tailed Spearman correlation test; $\alpha = 0.05$; $r = 0.50$, $p = 1.0$).

of the same data depicted the percentage of anaphase cells with spindle angles falling within each 10° increment from 0° to 90° (mean ± SE, n = 3 experiments).

Statistical Analyses

The Kolmogorov-Smirnov test was used to test the normality of data sample distributions. Most spindle angle data samples deviated from the Gaussian distribution. Thus, the nonparametric Mann-Whitney test (two-tailed test, $\alpha = 0.05$) was used to compare medians of samples. The nonparametric Spearman test (two-tailed test, $\alpha = 0.05$) was used to correlate sample parameters. All statistical analyses were performed using Prism software (GraphPad Software, San Diego, CA).

RESULTS

Cell Shape Does Not Correlate with Planar Spindle Orientation in Epithelial Monolayers

Because cell shape has been implicated in spindle orientation, we began by assessing whether this parameter might also influence spindle orientation in the Z-axis using Madin-Darby Canine Kidney II (MDCK II) epithelial monolayers (Figure 1a). Although polarized epithelia are often columnar, the geometry of mitotic cells, which undergo extensive cell rounding, has not been reported. If cell shape were responsible for the division plane, then changes in cell height-width ratios would be expected to alter spindle orientation. To obtain cells with different geometries, MDCK cells were grown on coverslips to different confluences or on polycarbonate transwell filters to high density. Mean cell height, cell width, and pole-to-pole spindle length of metaphase cells were measured and compared with the mean spindle angle of neighboring anaphase cells (Figure 1). Cell dimensions were taken in metaphase (Figure 1b), because this is when the spindle is at its longest before sister chromatid separation, and thus any geometric constraints on spindle movements would be expected to be at their greatest. Anaphase cells were used for spindle angle measurements to avoid inaccuracies resulting from spindle orientation changes during metaphase (Figure 1c).

We found no correlation between cell shape and mitotic spindle orientation in polarized epithelial sheets (Figure 1, d and e). In subconfluent monolayers, cell shape had the potential to constrain spindle orientation to some degree (Figure 1b), because cell height (8.2 ± 0.3 μm) in these flat cells was only slightly greater than the spindle length (7.9 ± 0.2 μm). However, cells grown on transwell filters were almost square (height-width ratio = 0.8), and the mean cell height (16.8 ± 0.2 μm) was far greater than spindle length (6.0 ± 0.1 μm). Despite this significant increase in cell height relative to width, the mean spindle angle relative to the plane of the monolayer was still <6° (Figure 1d). Moreover, there was no statistically significant correlation between metaphase cell height-width ratios and the orientation of the mitotic spindle in anaphase (Figure 1e). This implied that another mechanism must exist to orient spindles in polarized epithelial cells.

Cell–Cell Contact Is Necessary for Planar Spindle Orientation

When simple polarized epithelia prepare to divide, their mitotic spindles orient with their poles, and astral microtu-

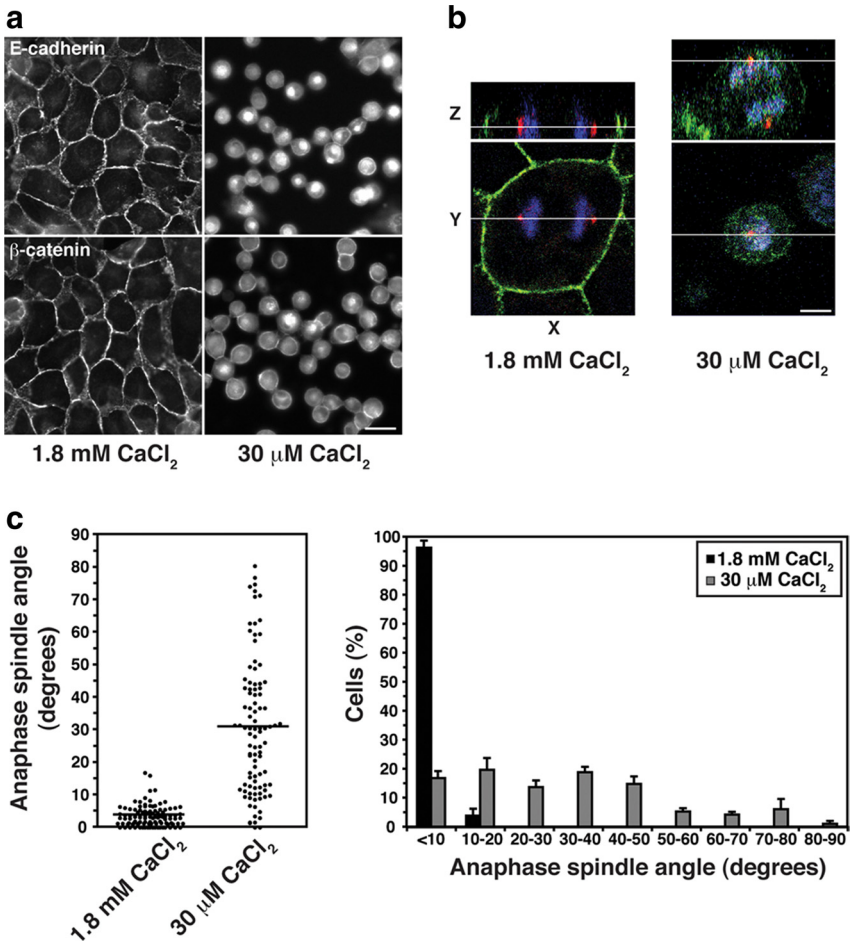

Figure 2. Spindles misorient when cell–cell contacts are disrupted. (a) Localization of E-cadherin and β-catenin in MDCK cells incubated in physiological (1.8 mM) or 30 μM $CaCl_2$ for 1.5 h to disrupt cell–cell contacts. Bar, 20 μm. (b) XY and XZ projections of confocal Z-stacks taken of anaphase cells stained for β-catenin (green), γ-tubulin (red), and DNA (blue). The anaphase cell in 30 μM $CaCl_2$ has not divided within the plane of the monolayer, in contrast to the cell in 1.8 mM $CaCl_2$. In this, and subsequent figures, apical is up and white lines indicate the planes at which orthogonal views were taken. Bar, 5 μm. (c) Anaphase spindle angles of cells incubated in 1.8 mM or 30 μM $CaCl_2$. For each condition, the spread and overall mean of spindle angles from three independent experiments, each with $n \geq 30$ cells, together with a frequency distribution of spindle angles (mean ± SE of the three experiments), are shown. Spindle orientation in the plane of the monolayer was perturbed by calcium depletion (two-tailed Mann-Whitney test, $p < 0.0001$).

bules are directed out toward the cell–cell contacts (Reinsch and Karsenti, 1994). Accordingly, components of the lateral membrane have long been regarded as attractive candidates to act as spatial cues for the spindles. However, the precise molecular identity of any such cues has not been definitively established.

To test whether cell–cell contact is necessary for the fidelity of Z-axis spindle orientation, we measured anaphase spindle angles in MDCK cells after their cell–cell interactions were disrupted by depleting extracellular calcium (Figure 2a). In contrast to intact controls, many anaphase spindle poles were found poking up above the plane of the monolayer when contacts were perturbed (Figure 2b). Although 96% of anaphase cells with intact cell–cell contacts divided with an angle <10° relative to the plane of the monolayer, this was reduced to only 17% in monolayers lacking cell–cell contacts (Figure 2c). This strongly suggested that cell–cell interactions can affect spindle orientation in simple epithelial monolayers.

Cell–cell contact concentrates many proteins at the lateral cortex (Rodriguez-Boulan and Nelson, 1989). We focused on a potential spindle orientation role for cadherin adhesion receptors, major determinants of epithelial cell–cell interactions, which accumulate at the lateral surface close to the spindles in our cells (Figure 1a) and in earlier studies (Reinsch and Karsenti, 1994). Moreover, asymmetric accumulation of cadherins and adherens junctions components is implicated in spindle orientation during asymmetric cell division (Le Borgne *et al.*, 2002; Yamashita *et al.*, 2003).

We therefore asked whether the impact of calcium chelation on spindle orientation involves cadherin adhesion (Figure 3). For this, we used the capacity of mAb SHE 78-7, directed against the ectodomain of human E-cadherin, to potently block adhesive binding (Kovacs *et al.*, 2002b). Because this mAb is species specific, we performed these studies in MCF10A cells, which form simple polarized monolayers in culture. We confirmed that chelation of extracellular calcium disrupts cell–cell contacts and misorients spindles in MCF10A cells as it does in MDCK cells (Figure 3, a–c). Further, we found that spindle orientation was corrected when cell–cell contact was restored by addition of extracellular calcium (Figure 3c). However, spindles remained misoriented when E-cadherin function was blocked with mAb SHE 78-7, despite restoration of extracellular calcium (Figure 3, b and c), being perturbed to the same extent as incubating cells in the absence of calcium. Therefore, preventing productive E-cadherin ligation blocked the ability of cells to correct spindle orientation even when calcium was restored.

DN-E-Cadherin Selectively Perturbs Planar Spindle Orientation

Cadherin adhesion supports many key aspects of epithelial biogenesis, including the integrity of cell–cell contacts (cohesion), assembly of specialized junctions (tight junctions, desmosomes), and apicobasal cell polarity (Takeichi, 1995). Although our observations suggested that E-cadherin might influence spindle orientation in mammalian epithelia, it remained possible that spindle misorientation was an indirect consequence of disrupting other aspects of epithelial organization. Similarly, although disruption of DE-cadherin also affects spindle orientation in *Drosophila* (Wang *et al.*, 2004),

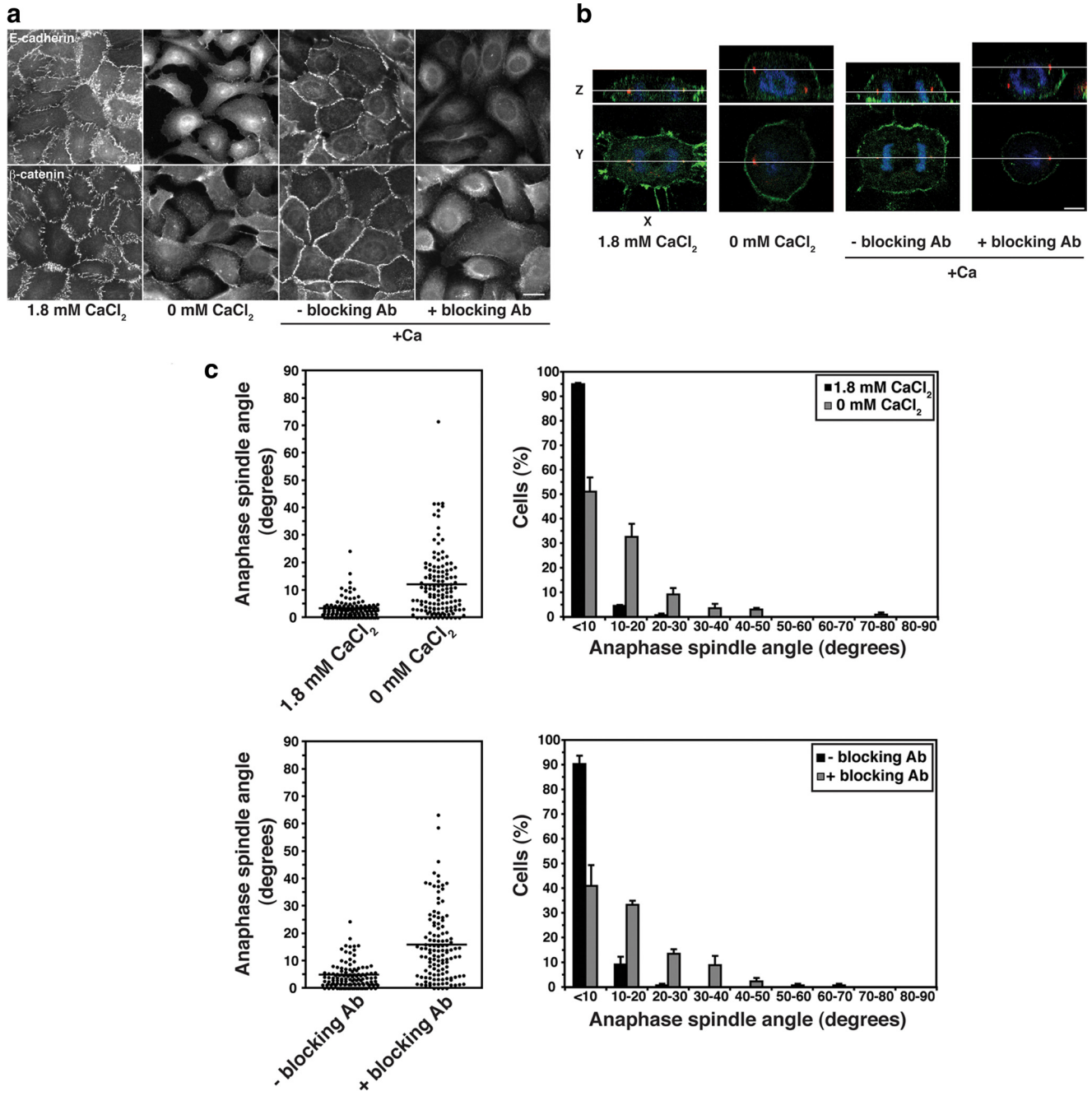

Figure 3. Spindles misorient when E-cadherin ligation is blocked. (a) E-cadherin and β-catenin staining in MCF10A cells incubated in physiological $CaCl_2$ (1.8 mM), in the absence of $CaCl_2$ for 2 h or in the presence or absence of E-cadherin antibody SHE78-7 for 5 h when $CaCl_2$ was restored after depletion to disrupt cell–cell contacts. Bar, 20 μm. (b) XY and XZ projections of anaphase cells stained for β-catenin (green), γ-tubulin (red), and DNA (blue). Anaphase cells from monolayers treated with 0 mM $CaCl_2$ or E-cadherin–blocking antibody have not divided within the plane of the monolayer, whereas control anaphase cells have. Bar, 5 μm. (c) Anaphase spindle angles of cells treated as in panel a. Data represented as in Figure 2. Both calcium depletion and E-cadherin blocking antibody affected spindle orientation (two-tailed Mann-Whitney tests, $p < 0.0001$).

whether this occurs independently of other morphogenetic effects of DE-cadherin remains an open question.

To pursue this question, we used a dominant-negative (DN) mutant of E-cadherin (GFP-DN E-cadherin; Figure 4a) consisting of the entire cytoplasmic tail expressed as a cytoplasmic protein. We performed these experiments in MDCK cells, which had the most dramatic response of spindle orientation to changes in cell–cell contact (Figure 2). Consistent with the ability of the cadherin tail alone to bind and stabilize catenins, total protein levels of both α- and β-catenin were elevated (Figure 4c), forming prominent cytoplasmic pools (Figure 4b). Total levels of endogenous E-cadherin were somewhat reduced (Figure 4c), and its junctional staining was significantly decreased (Figure 4b).

GFP-DN E-cadherin perturbed the orientation of the spindle. Over half the cells expressing GFP-DN E-cadherin

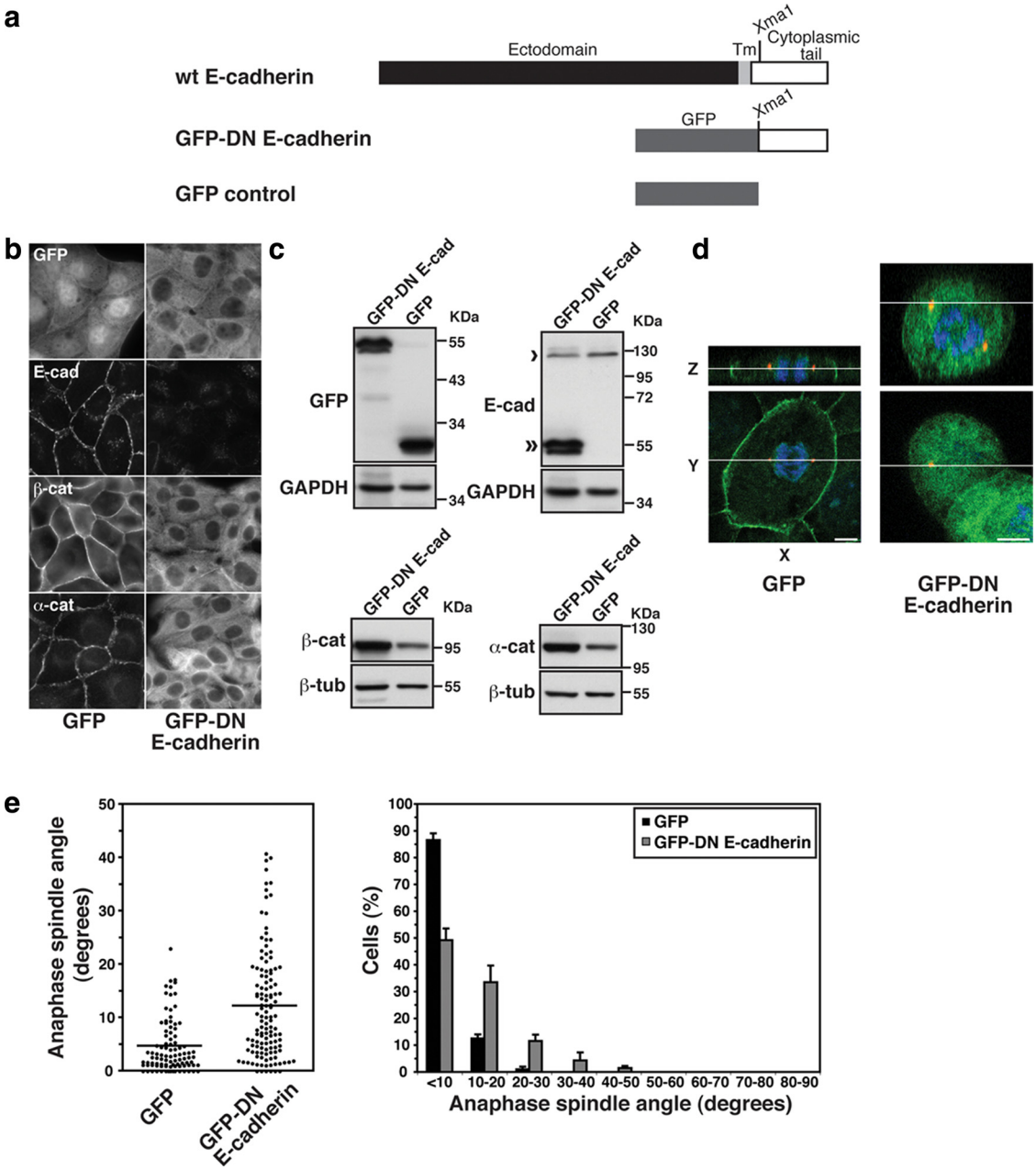

Figure 4. Cadherin acts as a spatial cue to orient the mitotic spindle independently of cell–cell cohesion. (a) Schematic diagram of a dominant-negative mutant of human E-cadherin. (b) Immunofluorescence characterization of E-cadherin and catenins in MDCK clones stably expressing GFP-DN E-cadherin or GFP protein alone. (c) Protein expression in MDCK clones stably expressing GFP-DN E-cadherin or GFP protein alone. Western blots of cell lysates were probed for GFP (identifying the transgenes), E-cadherin (identifying both endogenous protein [single arrow], and the mutant transgene [double arrow]), β-catenin, and α-catenin. GAPDH or β-tubulin were used as loading controls. (d) XY and XZ projections of anaphase cells stained for β-catenin (green), γ-tubulin (red), and DNA (blue). The anaphase cell expressing GFP-DN E-cadherin has not divided within the plane of the monolayer (XY); note also that the x-y confocal slice is taken high in the dividing cell, so that surrounding cells in the monolayer are not apparent. Bars, 5 μm. (e) Anaphase spindle angles of MDCK clones expressing GFP-DN E-cadherin or GFP. Data are represented as in Figure 2. For both GFP-DN E-cadherin and GFP, data from two clones, each of which gave similar results, were pooled. Spindle orientation was affected by expression of GFP-DN E-cadherin (two-tailed Mann-Whitney test, $p < 0.0001$).

showed anaphase spindle angles >10° from the plane of the monolayer, whereas the majority of control cells (87%) expressing GFP alone showed spindle angles <10% from the monolayer plane (Figure 3, d and e).

Importantly, cells with misoriented spindles preserved the integrity of their contacts with other cells, as demonstrated by staining for F-actin and desmosomes (desmoplakin), which showed no identifiable gaps in the monolayer (Figure 5a). Moreover, Na,K-ATPase remained localized to basolateral domains, whereas tight junctions (identified by claudin-4 and ZO-1) persisted at the apical interface between cells (Figure 5a); nor did GFP-DN E-cadherin significantly affect the localization of the polarity determinants Par3, aPKCζ, Lgl1, Dlg1, and Scribble (Figure 5b). This indicated that the ability of cadherin to control spindle orientation was not simply due to its

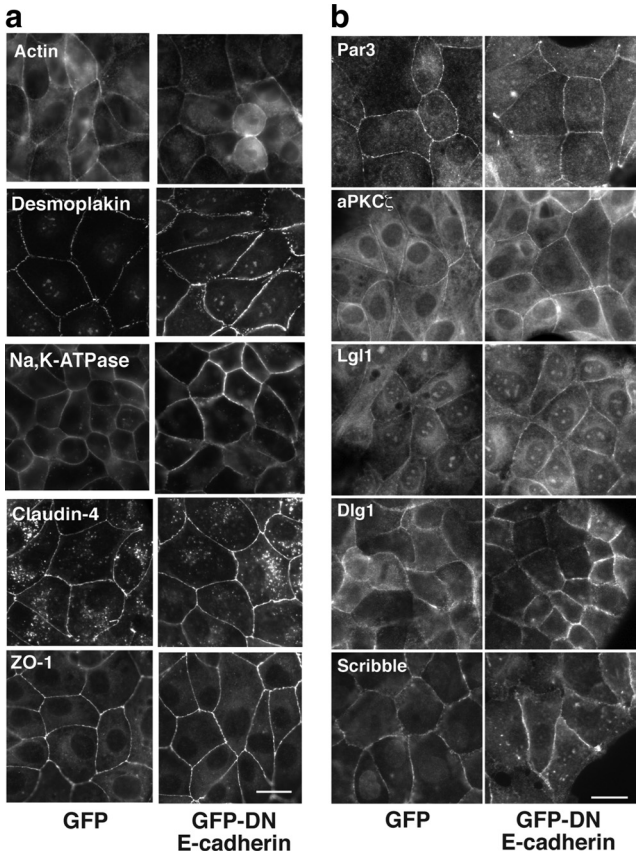

Figure 5. Dominant-negative cadherin does not disrupt cell–cell junctions or polarity determinants. Confluent MDCK monolayers stably expressing GFP-DN E-cadherin or GFP alone were examined by immunofluorescence microscopy. All experiments were performed under identical culture conditions and confluency as the experiments measuring spindle orientation. Two clones were analyzed for each construct, both of which gave comparable results. Scale bar, 20 μm. Monolayers were stained for junctional markers (a) or polarity determinants (b), as indicated.

ability to support cell–cell cohesion, junctional assembly, or cell polarity. Thus the impact of cadherin on spindle orientation appeared to be experimentally distinguishable from these other major functions of cadherin adhesion.

Homophilic Cadherin Ligation Directs Spindle Orientation in Nonpolarized Cells

Cadherin receptors could influence spindle orientation by themselves acting as cortical cues or by allowing other juxtacrine signals to be activated when adhesion brings cell surfaces together (Yap and Kovacs, 2003). Blocking antibody and dominant-negative strategies do not distinguish between these possibilities. Accordingly, we tested whether engagement of cellular cadherins using recombinant cadherin ligands could be sufficient to affect spindle orientation. We further reasoned that if cadherin receptors themselves provide instructive spatial cues to the spindle, then their ligation in a restricted region of the cortex should alter spindle orientation in otherwise unpolarized cells. To test this, we plated nonpolarized CHO cells stably expressing E-cadherin (hE-CHO) cells onto substrata coated with the recombinant cadherin ligand, hE/Fc, so that cadherin was only ligated on the basal surfaces of the cells (Figure 6). In earlier studies we showed that interphase hE-CHO cells adhere to hE/Fc in a cadherin-dependent manner, with no evidence of integrin signaling, and reorganize cadherin clusters and the cortical actin cytoskeleton at the basal surfaces that are in contact with the cadherin ligand (Kovacs *et al.*, 2002a,b; Scott *et al.*, 2006).

hE-CHO cells plated onto control coverslips divided horizontally, with a mean spindle angle of 3°, and with 94% of cells having a spindle angle $<10°$ from the plane of the substratum (Figure 6). In contrast, when hE-CHO cells were plated onto hE/Fc, the mean angle was increased fivefold, and the proportion of anaphase spindles within 10° of the substratum was substantially reduced. Indeed, a significant number of cells plated on hE/Fc showed spindle angles $>20°$ from the horizontal, which were not seen in controls. Thus, concentration of E-cadherin in a defined region of the cortex can alter spindle orientation in the Z-axis, a result that confirms the capacity of E-cadherin to act as an instructive spatial cue to influence mitotic spindle orientation. Interestingly, this effect of cadherin substrata on spindle orientation contrasts with that observed for integrin adhesion to matrix proteins, which preserves spindle orientation parallel to the substrate in isolated cells (Toyoshima and Nishida, 2007).

E-Cadherin and Cadherin-6 Exert Redundant Effects on Planar Spindle Orientation

We then tested whether controlling spindle orientation was a property specific to E-cadherin by exploiting the fact that MDCK cells express both E-cadherin and cadherin-6 (Stewart *et al.*, 2000). To our surprise, we found that depletion of E-cadherin by RNAi had no effect on spindle orientation (Figure 7, a, c, and d), nor did it disrupt cell–cell cohesion or the junctional localization of catenins (not shown), consistent with earlier reports of potential compensation by cadherin-6, a type II cadherin that also binds catenins (Figure 7b; Stewart *et al.*, 2000; Capaldo and Macara, 2007).

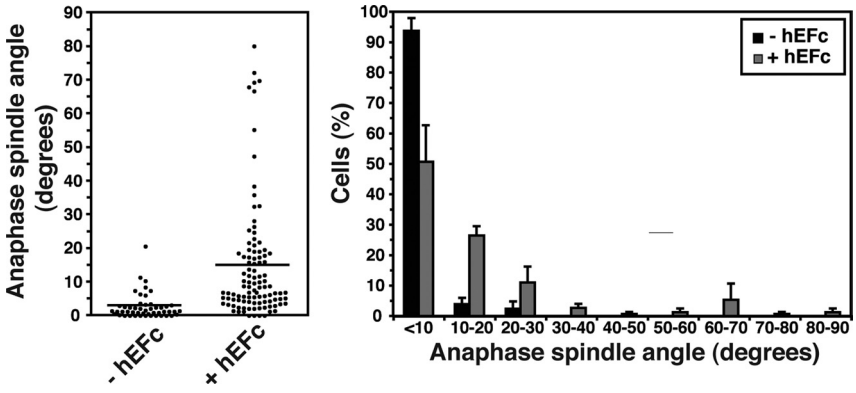

Figure 6. Localized cadherin homophilic ligation alters spindle orientation in nonpolarized cells. Anaphase spindle angles relative to the plane of the substratum of isolated hE-CHO cells plated for 1.5 h onto hE/Fc-coated or onto control coverslips (data pooled from three independent experiments, each with $n \geq 13$ cells). Plating cells onto E-cadherin ligand altered spindle orientation (two-tailed Mann-Whitney test, $p < 0.0001$).

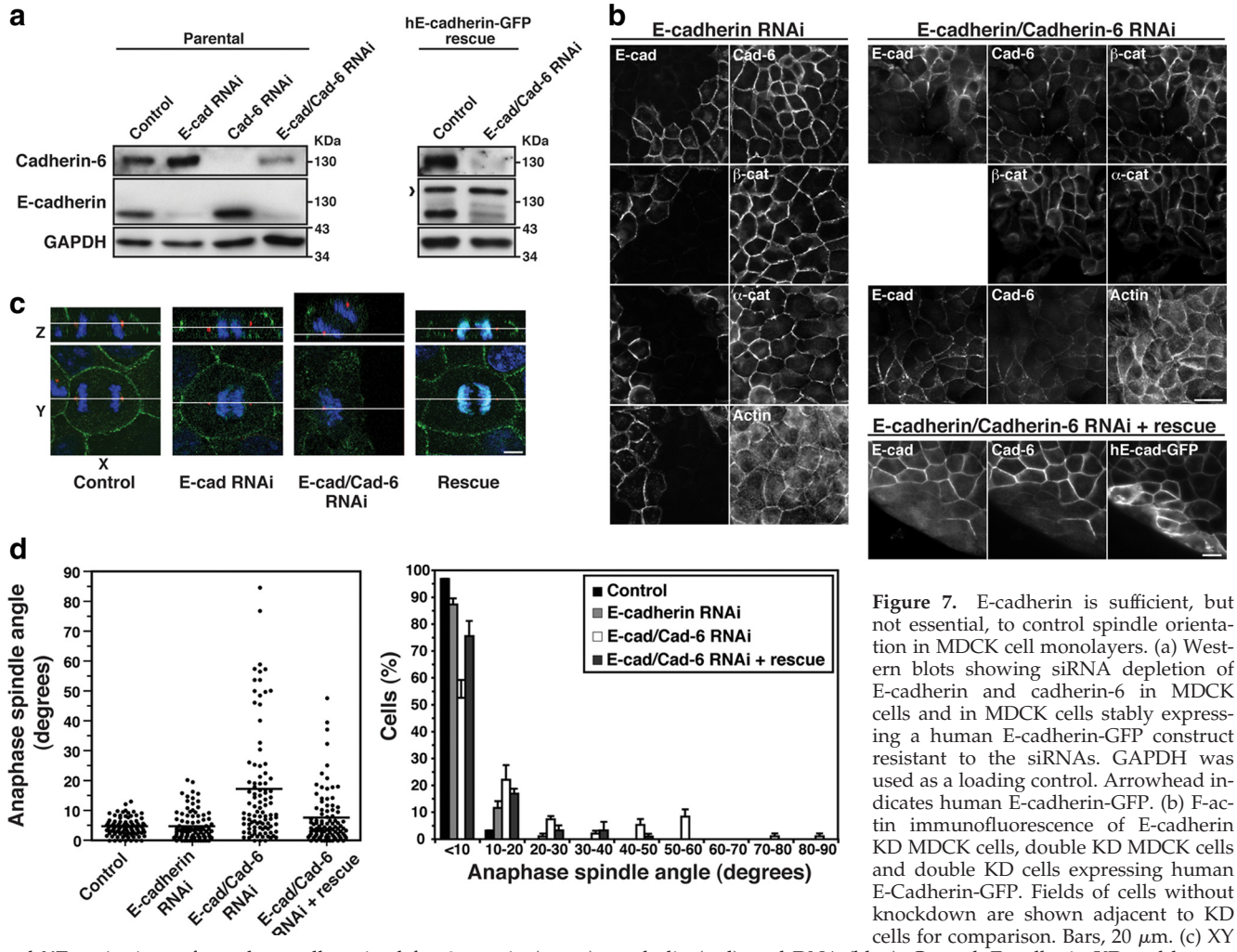

Figure 7. E-cadherin is sufficient, but not essential, to control spindle orientation in MDCK cell monolayers. (a) Western blots showing siRNA depletion of E-cadherin and cadherin-6 in MDCK cells and in MDCK cells stably expressing a human E-cadherin-GFP construct resistant to the siRNAs. GAPDH was used as a loading control. Arrowhead indicates human E-cadherin-GFP. (b) F-actin immunofluorescence of E-cadherin KD MDCK cells, double KD MDCK cells and double KD cells expressing human E-Cadherin-GFP. Fields of cells without knockdown are shown adjacent to KD cells for comparison. Bars, 20 μm. (c) XY and XZ projections of anaphase cells stained for β-catenin (green), γ-tubulin (red), and DNA (blue). Control, E-cadherin KD and human E-cadherin-GFP–expressing double KD cells have all divided within the plane of the monolayer, whereas the double KD MDCK cell has not. Bar, 5 μm. (d) Anaphase spindle angles of cells treated as in panel c. Data are represented as in Figure 2. Spindle orientation was not affected by E-cadherin KD alone (two-tailed Mann-Whitney test, $p > 0.05$), but was affected by KD of both E-cadherin and cadherin-6 ($p < 0.0001$). Correct spindle orientation in double KD cells was restored by expression of human E-cadherin-GFP ($p > 0.05$).

Spindle orientation was perturbed, however, in cells depleted of both E-cadherin and cadherin-6 by RNAi (Figure 7, a,c, and d). Z-axis orientation was restored in double knockdown (KD) cells expressing human E-cadherin-GFP, which was resistant to canine-specific siRNAs (Figure 7, c and d).

Again, it is noteworthy that monolayer cohesion was not disrupted by double cadherin KD (Figure 7b, F-actin staining), consistent with earlier reports (Capaldo and Macara, 2007). Overall, then, these findings confirm that cadherin receptors are required for planar spindle orientation in simple epithelia. They further indicate that although E-cadherin is sufficient to orient spindles, this property is shared with another catenin-binding cadherin. Whether other classical or type II cadherins also possess the capacity to orient spindles, as does cadherin-6, remains to be determined.

Junctional APC Correlates with Fidelity of Spindle Orientation

Finally, in order to gain insight into the molecular mechanism by which cadherins influence spindle orientation, we examined the effect of GFP-DN E-cadherin on cortical factors reported to influence spindle orientation in other contexts. Our aim in this screening was to identify substantive changes in protein localization in cells where cadherin function was targeted. We found no obvious change in localization of the mitotic spindle regulators NuMA and LGN (Du and Macara, 2004), nor in dynein IC or the dynactin subunit $p150^{Glued}$, which are implicated in spindle movements (O'Connell and Wang, 2000; Dujardin and Vallee, 2002) and could potentially link microtubule plus ends to β-catenin at junctions (Busson *et al.*, 1998; Ligon *et al.*, 2001; Figure 8).

However, we observed a striking effect of GFP-DN E-cadherin on the cortical localization of APC (Figure 9). Using two different antibodies, we found that APC consistently localized to the cell cortex at the apicolateral region of mitotic MDCK cells in the same Z-region as the mitotic spindle (Figure 9a). However, this cortical APC staining was lost in cells expressing GFP-DN E-cadherin (Figure 9b). Furthermore, junctional APC was preserved in cells depleted of E-cadherin alone, but was lost in double E-cadherin/cadherin-6 KD cells and restored by exogenous human E-cadherin-GFP (Figure 9b). Thus, these findings identify cadherin adhesion as a regulator of APC cortical localization

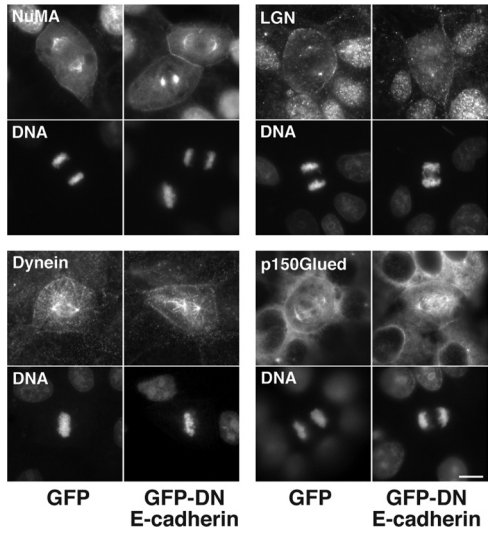

Figure 8. Cortical localization patterns of NuMA, LGN, dynein, and $p150^{Glued}$ in mitotic MDCK cells expressing GFP-DN E-cadherin or GFP. Cortical localization was not overtly perturbed by GFP-DN E-cadherin expression. All experiments were performed under identical culture conditions and confluency as the experiments measuring spindle orientation. Scale bar, 10 μm.

during mitosis and demonstrate that loss of junctional APC correlates strictly with conditions that perturb planar spindle orientation.

To test the potential significance of APC for planar spindle orientation, we depleted APC by siRNA (Figure 9, c and d). This largely abolished junctional staining of APC and substantially reduced total cellular levels assessed by Western blotting (Figure 9c). Spindle orientation was significantly perturbed in APC KD cells (Figure 9d). Although 84% of control cells displayed spindles $<5^{o}$ relative to the plane of the monolayer, the majority of APC KD cells (70%) showed spindle $>5^{o}$ from the plane of the monolayer. Thus depletion of APC induced planar spindle misorientation as had specific disruption of cadherin function.

DISCUSSION

Classical cadherins, such as E-cadherin, have long been acknowledged to exert profound effects on tissue morphogenesis (Tepass *et al.,* 2000). Their morphogenetic impact is likely mediated through multiple cellular mechanisms, including cell surface adhesion, cell–cell recognition and regulation of the actin cytoskeleton. Our present findings establish a novel mechanism for classical cadherins to affect tissue organization, by acting as cues that orient the mitotic spindle during symmetric cell divisions in mammalian epithelia.

We found that planar spindle orientation in simple polarized epithelia was consistently disrupted when cadherin function was perturbed. This is consistent with earlier reports from *Drosophila* and *Caenorhabditis elegans* that implicated adherens junction integrity as an important factor in spindle orientation. Many of those earlier studies, however, used indirect maneuvers (McCartney *et al.,* 2001), such as Crumbs mutants (Lu *et al.,* 2001), to perturb adherens junction integrity, rather than directly manipulating the cadherin itself. Moreover, although cadherins are important components of adherens junctions, they are not the only constituents of these junctions, which contain a range of other adhesion molecules, such as nectins (Takai *et al.,* 2008) and echinoid (Wei *et al.,* 2005), which have extensive impact on cell behavior. By using multiple techniques that specifically target cadherin function, including blocking antibodies, dominant-negative mutants and RNAi, our current experiments therefore allow us to extend these earlier studies to directly implicate cadherin receptors themselves in control of spindle orientation.

Of course, classical cadherins have diverse effects on epithelial organization, including maintenance of cell–cell cohesion, supporting other specialized junctions and apicobasal polarity. It was possible that the spindle misorientation that we observed arose as a consequence of these other effects of cadherins. Thus it is noteworthy that expression of the DN-E-cadherin mutant perturbed spindle orientation without overtly disrupting the cohesion of cell–cell contacts, other junctions or apicobasal polarity. Similarly, cell–cell cohesion was preserved in E-cadherin/cadherin-6 KD monolayers that misoriented their spindles. Although we cannot exclude subtle effects, these data strongly suggest that the ability of cadherin to influence planar spindle orientation may be a function experimentally distinguishable from its other major effects on epithelial organization. The notion that cadherin influences spindle orientation by serving as a spatial cue is reinforced by our demonstration that local ligation of cadherin receptors can reorient the spindle even in nonpolarized cells.

Identifying the molecular mechanism that allows cadherins to control spindle orientation will be an important challenge for the future. Among a range of potential cortical positioning factors that we screened, APC emerged as an interesting candidate to serve this function. APC has been identified as a spindle-positioning factor in *Drosophila* (Lu *et al.,* 2001; McCartney *et al.,* 2001; Yamashita *et al.,* 2003) and in isolated mammalian and yeast cells (Green *et al.,* 2005), although exceptions exist (McCartney *et al.,* 2006). We observed that APC localized at cell–cell junctions, as has been reported previously (Rosin-Arbesfeld *et al.,* 2001), and this junctional localization was lost when cadherin function was perturbed. Thus, loss of junctional APC correlated well with conditions that cause spindle misorientation. Moreover, depletion of cellular APC caused spindle misorientation akin to that seen when cadherin function was manipulated. This is further consistent with recent evidence of spindle misorientation in intestinal epithelial cells from $APC^{Min/+}$ mice (Fleming *et al.,* 2009).

These observations make APC an attractive candidate to mediate between cadherins and the mitotic spindle. However, it should be noted that APC can affect mitosis in other ways, which include altering spindle dynamics and microtubule attachment to kinetochores (McCartney and Nathke, 2008). To definitively test how cortical APC may mediate spindle orientation in response to cadherin, we will first need to understand how cadherins determine APC cortical localization in order to specifically ablate it. Our observation that junctional localization of APC was abolished both by dominant negative cadherin and cadherin knockdown implies an upstream role for cadherin receptors in the junctional localization of APC. However, although APC can bind β-catenin, this interaction is thought not to occur when β-catenin is associated with cadherins (Gottardi and Gumbiner, 2001). Indirect recruitment via the actin cytoskeleton has been suggested (Rosin-Arbesfeld *et al.,* 2001), but definitive molecular characterization of how APC localizes at cell–cell junctions remains an open issue.

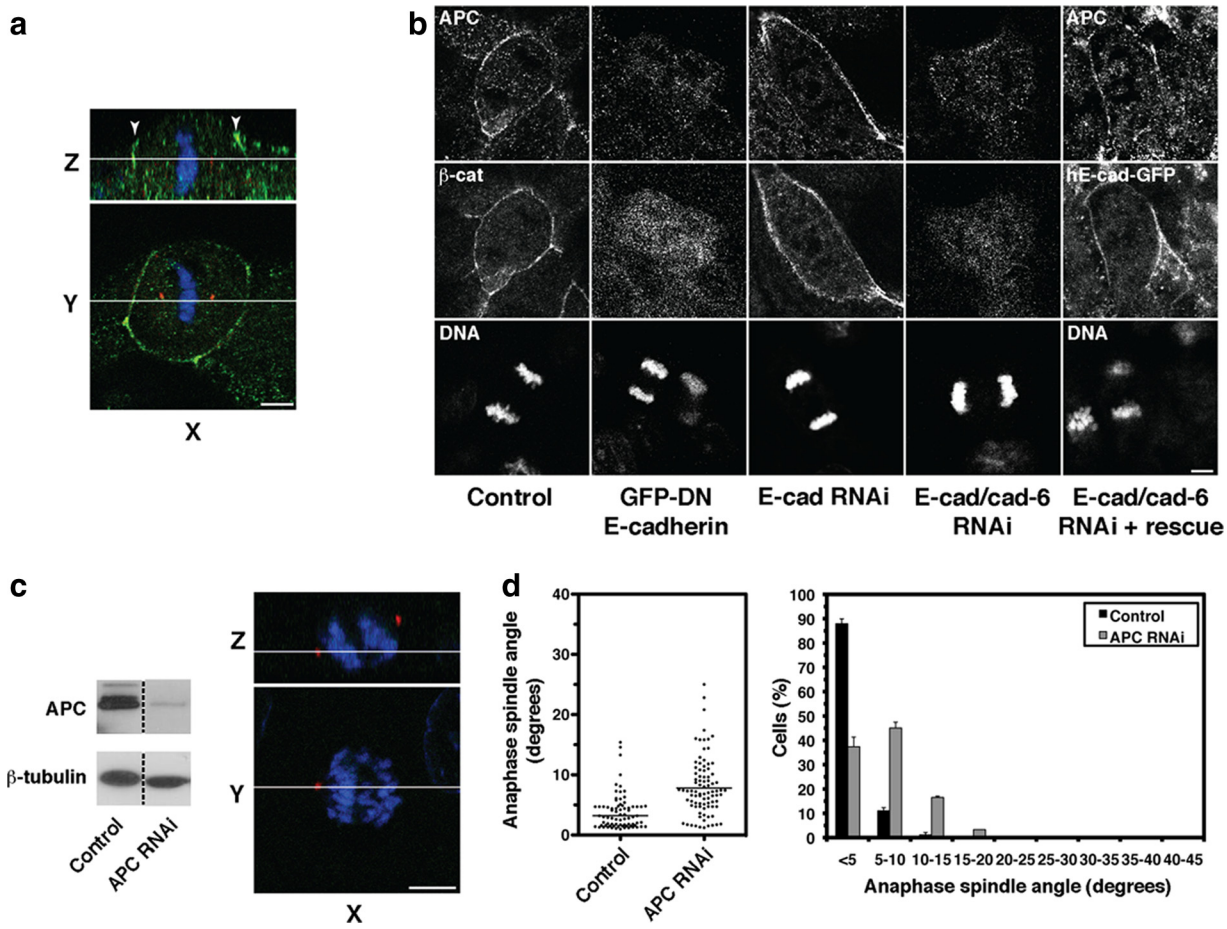

Figure 9. Loss of junctional APC correlates with conditions that cause spindle misorientation. (a) XY and XZ projections of a mitotic MDCK cell stained for APC (green), γ-tubulin (red), and DNA (blue). APC localized to the cortex in the same Z-region as the spindle poles. Arrowheads indicate apicolateral cortical staining of APC. Bar, 5 μm. (b) Localization of APC in MDCK cells treated with GFP-DN E-cadherin, E-cadherin RNAi, combined E-cadherin/cadherin-6 RNAi and double KD cells expressing human E-cadherin-GFP. For the rescue experiment, costaining for human E-cadherin-GFP is shown. In all other cases, costaining for β-catenin, whose loss from cell junctions also correlated with conditions that caused spindle misorientation, is shown. Bar, 5 μm. (c) Depletion of cellular APC by siRNA. APC levels following siRNA transfection were assessed by Western analysis in cell lysates and by immunofluorescence in mitotic cells. XY and XZ projections of anaphase cells stained for APC (green), γ-tubulin (red), and DNA (blue). Note loss of junctional APC staining in APC RNAi cells. (d) Anaphase spindle angles of control and APC RNAi MDCK cells. Data represented as in Figure 2 and pooled from three independent experiments (each with $n \geq 30$). Spindle orientation was affected by APC RNAi (two-tailed Mann-Whitney test, $p < 0.0001$).

Overall, then, we conclude that classical cadherin receptors serve as orientation cues to ensure the fidelity of planar spindle orientation in simple epithelia.

Cell–cell adhesion is not the only potential determinant of spindle orientation. Indeed, other factors, such as integrin adhesion or cell shape, presumably account for the ability of CHO cells to orient their spindles parallel to substrata in the absence of a cadherin cue. However, although integrins can orient spindles (Lechler and Fuchs, 2005; Toyoshima and Nishida, 2007), in our experiments cadherin disruption caused spindle misorientation without interfering with cell–substrate interactions. Moreover, although cell shape can direct x-y orientation of spindles in isolated cells (O'Connell and Wang, 2000), we found that spindle orientation in the Z-axis did not correlate with changes in cell height-width ratio, the shape parameter predicted to potentially affect spindle orientation in the Z-axis. We therefore propose that, when cells integrate into sheets, cadherins becomes key determinants of spindle orientation during symmetric cell division. Because asymmetric location of cadherins or adherens junctions also contributes to asymmetric spindle orientation (Le Borgne *et al.*, 2002), our findings point to a more general impact of cadherin adhesion receptors on spindle orientation during morphogenesis.

ACKNOWLEDGMENTS

We thank I. Nathke, P. Brennwald, M. Caplan, D. Compton, Q. Du, K. Green, B. Gumbiner, P. Humbert, R. M. Mège and K. Vaughan for antibodies. We are grateful to P. Humbert and H. Richardson (Peter MacCallum Cancer Centre) for helpful discussions and sharing reagents, and to J. Pines for advice and critical review of the manuscript. We also thank all our colleagues in the lab for their unfailingly generous support, especially Samantha Stehbens for her help with image processing. This work was funded by the National Health and Medical Research Council of Australia (NHMRC). A.S.Y. is an NHMRC Senior Research Fellow. NdE was supported by an NHMRC Peter Doherty Fellowship and a UQ Post-doctoral Fellowship. Confocal microscopy was performed at the ACRF/IMB Dynamic Imaging Centre for Cancer Biology, established with the generous support of the Australian Cancer Research Foundation.

REFERENCES

Ahringer, J. (2003). Control of cell polarity and mitotic spindle positioning in animal cells. Curr. Opin. Cell Biol. *15*, 73–81.

Baena-Lopez, L. A., Baonza, A., and Garcia-Bellido, A. (2005). The orientation of cell divisions determines the shape of *Drosophila* organs. Curr. Biol. *15*, 1640–1644.

Betschinger, J., and Knoblich, J. A. (2004). Dare to be different: asymmetric cell division in *Drosophila, C. elegans* and vertebrates. Curr. Biol. *14*, R674–685.

Busson, S., Dujardin, D., Moreau, A., Dompierre, J., and De Mey, J. R. (1998). Dynein and dynactin are localized to astral microtubules and at cortical sites in mitotic epithelial cells. Curr. Biol. *8*, 541–544.

Capaldo, C. T., and Macara, I. G. (2007). Depletion of E-cadherin disrupts establishment but not maintenance of cell junctions in Madin-Darby canine kidney epithelial cells. Mol. Biol. Cell *18*, 189–200.

Doe, C. Q., and Bowerman, B. (2001). Asymmetric cell division: fly neuroblast meets worm zygote. Curr. Opin. Cell Biol. *13*, 68–75.

Du, Q., and Macara, I. G. (2004). Mammalian Pins is a conformational switch that links NuMA to heterotrimeric G proteins. Cell *119*, 503–516.

Dujardin, D. L., and Vallee, R. B. (2002). Dynein at the cortex. Curr. Opin. Cell Biol. *14*, 44–49.

Fleming, E. S., Temchin, M., Wu, Q., Maggio-Price, L., and Tirnauer, J. S. (2009). Spindle misorientation in tumors from APC(min/+) mice. Mol. Carcinog. *48*, 592–598.

Fleming, E. S., Zajac, M., Moschenross, D. M., Montrose, D. C., Rosenberg, D. W., Cowan, A. E., and Tirnauer, J. S. (2007). Planar spindle orientation and asymmetric cytokinesis in the mouse small intestine. J. Histochem. Cytochem. *55*, 1173–1180.

Gottardi, C. J., and Gumbiner, B. M. (2001). Adhesion signaling: how b-catenin interacts with its partners. Curr. Biol. *11*, R792–R794.

Green, R. A., Wollman, R., and Kaplan, K. B. (2005). APC and EB1 function together in mitosis to regulate spindle dynamics and chromosome alignment. Mol. Biol. Cell *16*, 4609–4622.

Grohmann, A., Tanneberger, K., Alzner, A., Schneikert, J., and Behrens, J. (2007). AMER1 regulates the distribution of the tumor suppressor APC between microtubules and the plasma membrane. J. Cell Sci. *120*, 3738–3747.

Kaltschmidt, J. A., and Brand, A. H. (2002). Asymmetric cell division: microtubule dynamics and spindle asymmetry. J. Cell Sci. *115*, 2257–2264.

Kovacs, E. M., Ali, R. G., McCormack, A. J., and Yap, A. S. (2002a). E-cadherin homophilic ligation directly signals through Rac and phosphatidylinositol 3-kinase to regulate adhesive contacts. J. Biol. Chem. *277*, 6708–6718.

Kovacs, E. M., Goodwin, M., Ali, R. G., Paterson, A. D., and Yap, A. S. (2002b). Cadherin-directed actin assembly: E-cadherin physically associates with the Arp2/3 complex to direct actin assembly in nascent adhesive contacts. Curr. Biol. *12*, 379–382.

Le Borgne, R., Bellaiche, Y., and Schweisguth, F. (2002). *Drosophila* E-cadherin regulates the orientation of asymmetric cell division in the sensory organ lineage. Curr. Biol. *12*, 95–104.

Lechler, T., and Fuchs, E. (2005). Asymmetric cell divisions promote stratification and differentiation of mammalian skin. Nature *437*, 275–280.

Ligon, L. A., Karki, S., Tokito, M., and Holzbaur, E. L. (2001). Dynein binds to beta-catenin and may tether microtubules at adherens junctions. Nat. Cell Biol. *3*, 913–917.

Lu, B., Roegiers, F., Jan, L. Y., and Jan, Y. N. (2001). Adherens junctions inhibit asymmetric division in the *Drosophila* epithelium. Nature *409*, 522–525.

McCartney, B. M., McEwen, D. G., Grevengoed, E., Maddox, P., Bejsovec, A., and Peifer, M. (2001). *Drosophila* APC2 and Armadillo participate in tethering mitotic spindles to cortical actin. Nat. Cell Biol. *3*, 933–938.

McCartney, B. M., and Nathke, I. S. (2008). Cell regulation by the Apc protein: Apc as a master regulator of epithelia. Curr. Op. Cell Biol. *20*, 186–193.

McCartney, B. M., Price, M. H., Webb, R. L., Hayden, M. A., Holot, L. M., Zhou, M., Bejsovec, A., and Peifer, M. (2006). Testing hypotheses for the functions of APC family proteins using null and truncation alleles in *Drosophila*. Development *133*, 2407–2418.

Miranda, K. C., Khromykh, T., Christy, P., Le, T. L., Gottardi, C. J., Yap, A. S., Stow, J. L., and Teasdale, R. D. (2001). A dileucine motif targets E-cadherin to the basolateral cell surface in Madin-Darby canine kidney and LLC-PK1 epithelial cells. J. Biol. Chem. *276*, 22565–22572.

O'Connell, C. B., and Wang, Y. L. (2000). Mammalian spindle orientation and position respond to changes in cell shape in a dynein-dependent fashion. Mol. Biol. Cell *11*, 1765–1774.

Rappaport, R. (1971). Cytokinesis in animal cells. Int. Rev. Cytol. *31*, 169–213.

Reinsch, S., and Karsenti, E. (1994). Orientation of spindle axis and distribution of plasma membrane proteins during cell division in polarized MDCKII cells. J. Cell Biol. *126*, 1509–1526.

Rodriguez-Boulan, E., and Nelson, W. J. (1989). Morphogenesis of the polarized epithelial cell phenotype. Science *245*, 718–725.

Roegiers, F., and Jan, Y. N. (2004). Asymmetric cell division. Curr. Opin. Cell Biol. *16*, 195–205.

Rosin-Arbesfeld, R., Ihrke, G., and Bienz, M. (2001). Actin-dependent membrane association of the APC tumour suppressor in polarized mammalian epithelial cells. EMBO J. *20*, 5929–5939.

Scott, J. A., Shewan, A. M., den Elzen, N. R., Loureiro, J. J., Gertler, F. B., and Yap, A. S. (2006). Ena/VASP proteins can regulate distinct modes of actin organization at cadherin-adhesive contacts. Mol. Biol. Cell *17*, 1085–1095.

Stewart, D. B., Barth, A. I., and Nelson, W. J. (2000). Differential regulation of endogenous cadherin expression in Madin-Darby canine kidney cells by cell-cell adhesion and activation of beta -catenin signaling. J. Biol. Chem. *275*, 20707–20716.

Takai, Y., Ikeda, W., Ogita, H., and Rikitake, Y. (2008). The immunoglobulin-like cell adhesion molecule nectin and its associated protein afadin. Annu. Rev. Cell Dev. Biol. *24*, 309–342.

Takeichi, M. (1995). Morphogenetic roles of classic cadherins. Curr. Opin. Cell Biol. *7*, 619–627.

Tepass, U., Truong, K., Godt, D., Ikura, M., and Peifer, M. (2000). Cadherins in embryonic and neural morphogenesis. Nat. Rev. Mol. Cell Biol. *1*, 91–100.

Thery, M., and Bornens, M. (2006). Cell shape and cell division. Curr. Opin. Cell Biol. *18*, 648–657.

Thery, M., Jimenez-Dalmaroni, A., Racine, V., Bornens, M., and Julicher, F. (2007). Experimental and theoretical study of mitotic spindle orientation. Nature *447*, 493–496.

Thery, M., Racine, V., Pepin, A., Piel, M., Chen, Y., Sibarita, J. B., and Bornens, M. (2005). The extracellular matrix guides the orientation of the cell division axis. Nat. Cell Biol. *7*, 947–953.

Toyoshima, F., and Nishida, E. (2007). Integrin-mediated adhesion orients the spindle parallel to the substratum in an EB1- and myosin X-dependent manner. EMBO J. *26*, 1487–1498.

Wang, F., Dumstrei, K., Haag, T., and Hartenstein, V. (2004). The role of DE-cadherin during cellularization, germ layer formation and early neurogenesis in the *Drosophila* embryo. Dev. Biol. *270*, 350–363.

Wei, S. Y., *et al.* (2005). Echinoid is a component of adherens junctions that cooperates with DE-Cadherin to mediate cell adhesion. Dev. Cell *8*, 493–504.

Yamashita, Y. M., Jones, D. L., and Fuller, M. T. (2003). Orientation of asymmetric stem cell division by the APC tumor suppressor and centrosome. Science *301*, 1547–1550.

Yap, A. S., and Kovacs, E. M. (2003). Direct cadherin-activated cell signaling: a view from the plasma membrane. J. Cell Biol. *160*, 11–16.